Radiopharmaceuticals

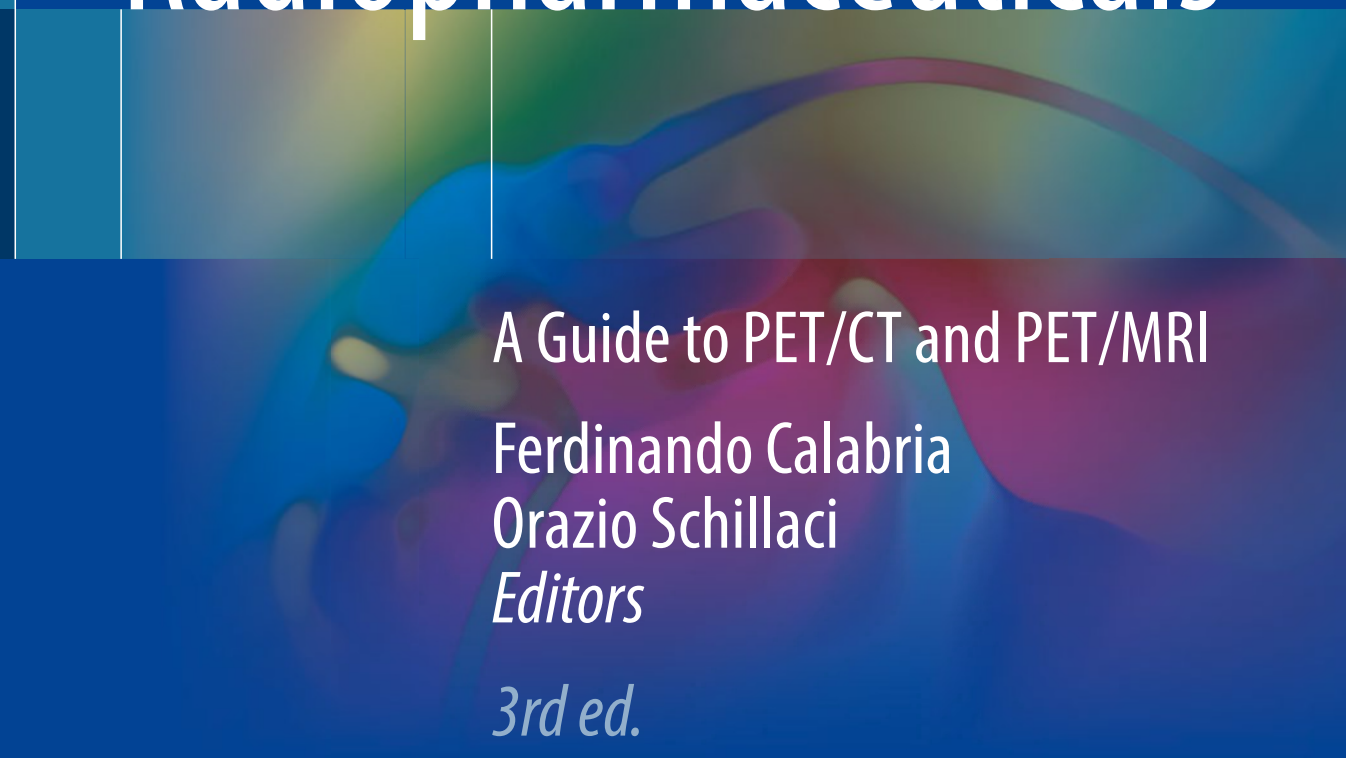

A Guide to PET/CT and PET/MRI

Ferdinando Calabria
Orazio Schillaci
Editors

3rd ed.

Springer

Radiopharmaceuticals

Ferdinando Calabria • Orazio Schillaci
Editors

Radiopharmaceuticals

A Guide to PET/CT and PET/MRI

3rd ed. 2024

Springer

Editors
Ferdinando Calabria
Department of Nuclear Medicine and Theranostics
Mariano Santo Hospital
Cosenza, Italy

Orazio Schillaci
Department of Biomedicine and Prevention
University of Rome Tor Vergata
Rome, Italy

ISBN 978-3-031-54195-7 ISBN 978-3-031-54196-4 (eBook)
https://doi.org/10.1007/978-3-031-54196-4

predecessor edition: Radiopharmaceuticals Ed:2, English, 2020.

This Springer imprint is published by the registered company Springer Nature Switzerland AG
The registered company address is: Gewerbestrasse 11, 6330 Cham, Switzerland

The dedication by Orazio Schillaci:
To Nicoletta, Maria Beatrice, and Agnese Felicia.
The dedication by Ferdinando Calabria:
To Rosario, my father.

Preface

Three years have passed since the publication of the previous edition, and we humbly must express our gratitude to the readers who have chosen this book as a resource for their learning process. This newly revised book aims to provide readers with an accessible, usable, and concise atlas guide to PET molecular imaging. Additionally, we appreciate the compliments from our peers. Conversely, we have the urge to add to its content in order to keep it useful in the broad field of PET molecular imaging.

Nuclear medicine is a discipline intrinsically based on the properties of these biological molecules; therefore, with the precious help of many Italian and European colleagues, the current edition of the book is expanded to cover further important chapters, from the imaging of prostate cancer with ^{18}F-fluciclovine, to new intriguing applications of radiolabeled FAPI and ^{18}F-fluoroestradiol, a further amino acid tracer as the ^{18}F-fluorothymidine, and the ^{68}Ga-Pentixafor, the tracer for imaging the chemokine receptor involved in tumor growth.

Some *old* chapters have been updated, in particular, due to the recent applications of radiolabeled choline, ^{18}F-DOPA, ^{68}Ga-PSMA, and ^{18}F-NaF; other chapters are kept in the new edition, for the peculiarities of, *in primis,* the ^{18}F-FDG and, consequently, ^{11}C-methionine, somatostatin receptor analogs, ^{18}F-FET, ^{64}Cu-radiopharmaceuticals, amyloid tracers, ^{82}Rb, ^{223}Ra-dichloride, and τ tracers. It is noteworthy to state that some of these diagnostic tracers represent the essential step in theranostics, while other agents enlarged the field of applications of PET to neurology and cardiology. Moreover, two additional chapters concern neuroinflammation imaging with TSPO agents and the hypoxia pathway with ^{18}F-FAZA.

This book now includes 30 PET radiopharmaceuticals, with more than 250 clinical cases demonstrating their diagnostic characteristics. Because it is yet unknown what the perfect radiopharmaceutical in nuclear medicine would be, the authors also discuss physiological variations in distribution and diagnostic problems related to particular biochemical pathways.

As in the past version, the authors describe the molecular pathway, biodistribution, physiopathology, and kinetics of each radiopharmaceutical, as the basis of the diagnostic role. The essential diagnostic features and the most common clinical indications are discussed for each tracer. Therefore, in this new version of the book, nuclear physicians, radiologists, and young colleagues will also find a friendly guide to the interpretation of PET images with the most important diagnostic tracers actually in use. Once again, we

know that this is a provisional list of PET tracers; at the same time, we are pleased about this because it represents the mirror image of the vitality of our discipline.

The goal of the work is still to assist professionals in their approach to a certain topic. In our opinion, the key for young nuclear physicians in understanding the landscape of PET imaging should be this synthesis between the data offered by clinicians and researchers and the reader's point of view. This *synthesis* should be taken into account in its truest sense: from the ancient Greek σύνθεσις (*súnthesis*), which is the result of "putting together" something coherent and comprehensive by combining simpler things. Because of the ongoing process of innovation, a scientist cannot claim to know everything; instead, they must strive to know as much as they can. For this purpose, we sincerely thank colleagues, researchers, and scientists who helped us to write the book, particularly in collecting clinical cases, describing diagnostic molecules, and synthesizing a large amount of data to provide the reader with a quick guide to PET molecular imaging.

Cosenza, Italy — Ferdinando Calabria
Rome, Italy — Orazio Schillaci

Contents

^{18}F-FDG

1

Ferdinando Calabria, Andrea Cimini, Antonio Bagnato, Domenico Gullà, Giuseppe L. Cascini, Nicoletta Urbano, and Orazio Schillaci

Abbreviations

^{18}F-FDG	^{18}F-Fluoro-deoxyglucose
BOLD	Blood oxygenation level dependent
FLAIR	Fluid attenuation inversion recovery
MIP	Maximum intensity projection
MRI	Magnetic resonance imaging
PET/CT	Positron emission tomography/computed tomography
ROI	Region of interest
SPECT/CT	Single photon emission computed tomography/computed tomography
SUVmax	Maximum standardized uptake value

F. Calabria (✉) · A. Bagnato
Department of Nuclear Medicine and Theranostics, Mariano Santo Hospital, Cosenza, Italy

A. Cimini
Department of Diagnostic Imaging, Molecular Imaging, Interventional Radiology and Radiotherapy, University Hospital Tor Vergata, Rome, Italy

D. Gullà
Neuroimaging PET/MRI Research Unit, Institute of Molecular Bioimaging and Physiology, Italian National Research Council, IBFM-CNR, Catanzaro, Italy

G. L. Cascini
Nuclear Medicine Unit, Department of Diagnostic Imaging, Magna Graecia University, Catanzaro, Italy

N. Urbano
Nuclear Medicine Unit, University Hospital "Tor Vergata", Rome, Italy

O. Schillaci
Department of Biomedicine and Prevention, University of Rome Tor Vergata, Rome, Italy

1.1 Synthesis

^{18}F-FDG is a glucose analog with the hydroxyl group on the 2-carbon of a glucose molecule replaced by ^{18}F, a β+ emitter isotope of fluorine. ^{18}F-FDG can be synthesized by either electrophilic or nucleophilic fluorination reactions. The first synthesis of ^{18}F-FDG was obtained in 1976 by electrophilic fluorination [1]. Instead, the chemical reaction of nucleophilic substitution involves the addition of a nucleophilic molecule (a negatively charged molecule) into a molecule with a leaving group (electron drawing group attached to the parent molecule through an unstable chemical bond). Nucleophilic fluorination, using mannose triflate as precursor and tetrabutylammonium salts, is largely used because of the high yield and short reaction time [2]. The main quality control requirements of ^{18}F-FDG regard the identity of radionuclide, radiochemical purity, pH, residual solvent, sterility, and the level of bacterial endotoxin. These tests should be finished after the tracer can be released [2].

F. Calabria, O. Schillaci (eds.), *Radiopharmaceuticals*,
https://doi.org/10.1007/978-3-031-54196-4_1

1.2 Pharmacokinetics

Being an analog of glucose, the ^{18}F-FDG plays an undisputed role in PET imaging, due to its versatility as marker of cellular metabolism. ^{18}F-FDG enters the cell by the same membrane transport mechanism as glucose. After penetration of the cellular membrane via glucose transporters [3], both ^{18}F-FDG and glucose are phosphorylated by hexokinase. Unlike glucose-6-phosphate, ^{18}F-FDG-6-phosphate is not a substrate of glucose-6-phosphate isomerase and does not undergo further metabolism in the glucose pathway. Therefore, ^{18}F-FDG remains trapped within cells (Fig. 1.1). The increased glucose utilization in tumor cells is due to three main reasons: overexpression of membrane glucose transporters, increased hexokinase activity, and decreased levels of glucose-6-phosphatase [4].

Physiologically, the tracer is taken up in cells with high metabolism or gradient of glucose uptake, as in the brain. First studies on ^{14}C-deoxgyglucose as imaging agent well displayed that synapses metabolism is strictly related with neuronal cells metabolism [5].

Subsequently, the ^{18}F-FDG has been successfully employed as tumor imaging marker, since it provides useful functional information based on the increased glucose uptake and glycolysis of cancer cells. Moreover, after the antiblastic therapy, this tracer can be considered as marker of response to therapy, owing to show the decrease in glucose metabolism in cancer cells, after therapy.

The clearance of ^{18}F-FDG is rapid and involves the renal system, through a filtration process of ^{18}F-FDG from blood pool into kidneys and a rapid production of radioactive urine, starting few minutes after the intravenous administration.

1.3 Physiological Distribution

The physiological distribution of ^{18}F-FDG concerns organs or tissues with high rate of glucose metabolism: in the brain, this radiopharmaceutical is normally taken up in the normal structures of gray matter, basal ganglia, cerebellum, and thalamus. A lower uptake gradient can be observed in the glial cells of the white matter, rectus muscle of the eye, medial and lateral, can show tracer uptake due to physiologic activity.

The myocardium normally can show high ^{18}F-FDG uptake, with a certain variability, since glucose is not the primary metabolic substrate of the myocardium. Due to the high affinity of the retic-

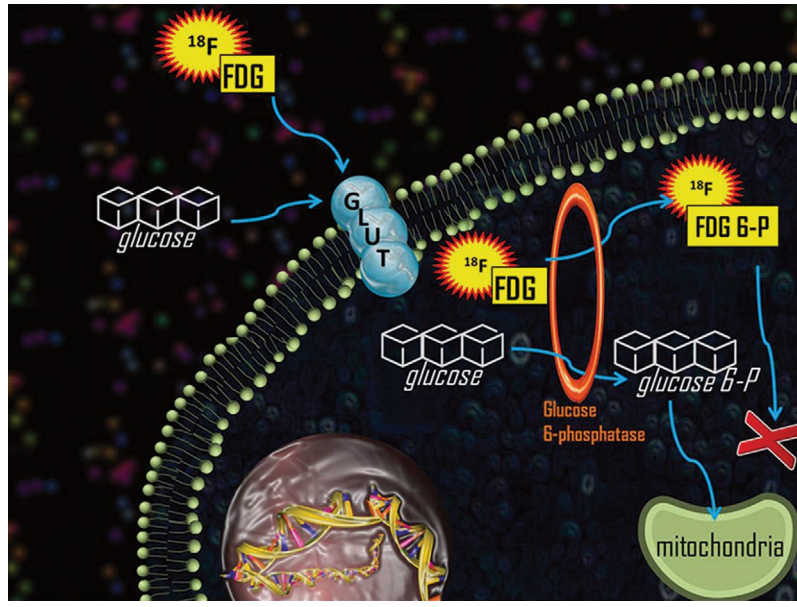

Fig. 1.1 Being an analog of glucose, the ^{18}F-FDG is internalized in cells and phosphorylated

uloendothelial cells, spleen and bone marrow are usually characterized by mild uptake. The liver usually shows high gradient of uptake, while kidneys, ureters, and bladder are normally visualized at PET imaging, due to the tracer renal excretion (Fig. 1.2). A certain grade of vascular activity can also be observed, especially for early imaging, in mediastinal vascular structures or in the iliac arteries. Finally, other sites of mild uptake are salivary and lachrymal glands, pancreas, stomach, and, due to the peristaltic activity, the intestinal loops, with large intra-individual variability.

Some physiopathological features of bio-distribution of the ^{18}F-FDG should be primarily considered the possibility of a diffuse homogeneous bone marrow uptake, which usually reflects hyperplastic bone marrow which can be documented in patients undergoing chemotherapy (Fig. 1.3).

Several methods are available for measuring the rate of ^{18}F-FDG accumulation in tissues. PET scanners are designed to measure the in vivo

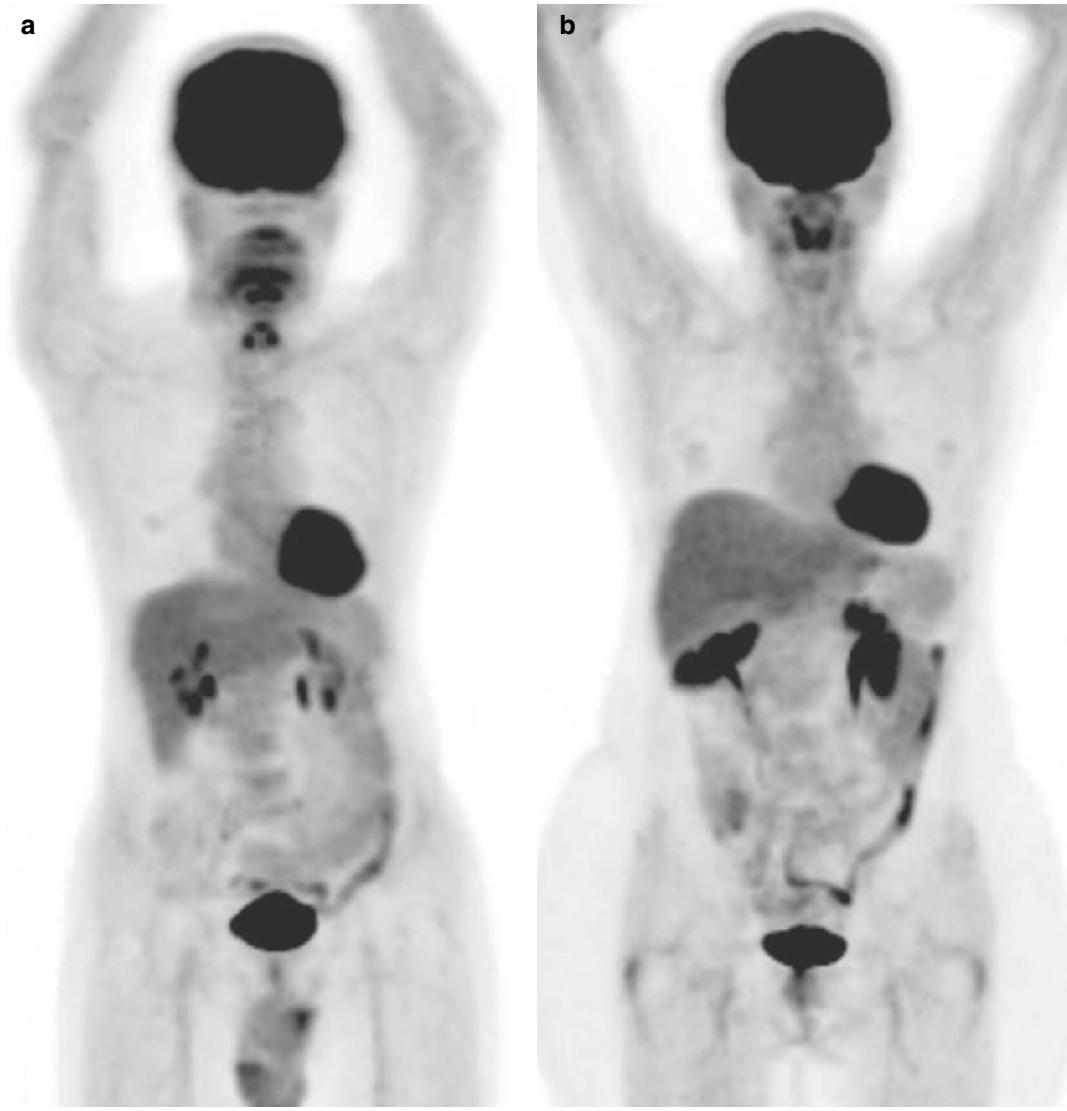

Fig. 1.2 Physiological whole body ^{18}F-FDG bio-distribution in a 42-year-old male subject (**a**) and a 36-year-old female subject (**b**)

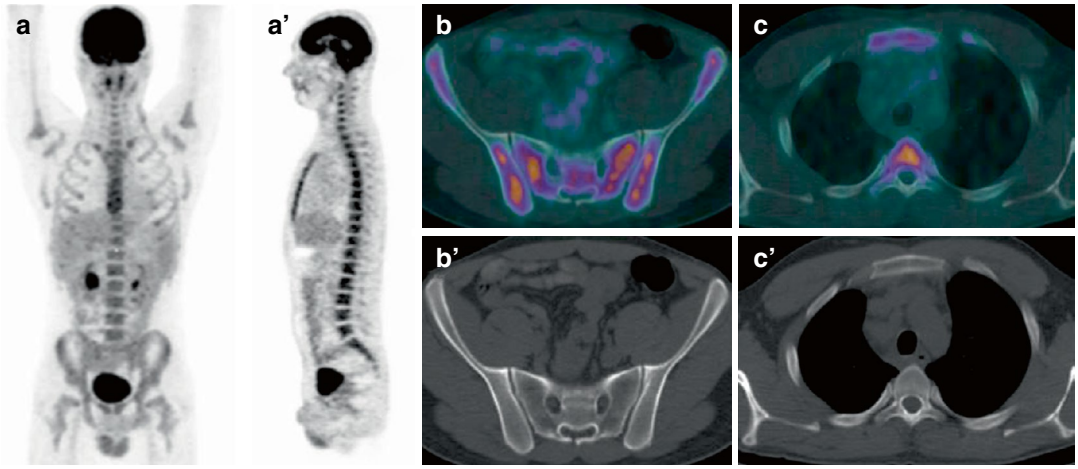

Fig. 1.3 ^{18}F-FDG 3D PET maximum intensity projection in coronal (**a**) and lateral (**a′**) views shows diffuse physiological uptake in the skeleton of a 45-year-old woman, due to bone marrow activation, 15 days after the end of chemotherapy. As evident in axial PET/CT (**b**, **c**) and CT (**b′**, **c′**) details, no morphological abnormalities are associated with functional findings

radioactivity concentration (kBq/mL), which is directly linked to the tracer concentration. However, it is the relative tissue uptake of ^{18}F-FDG that is of interest. The two most significant sources of variation that occur in practice are the amount of injected ^{18}F-FDG and the patient size. To compensate for these variations, the standardized uptake value (SUV) is used as a relative measure of ^{18}F-FDG uptake as it represents the most commonly used semiquantitative parameter for analysis of oncology PET studies.

The SUV is a semiquantitative value expressing degree of metabolic activity in selected tissues [6], by using a region of interest (ROI), and can be obtained by the following formula:

$$\mathrm{SUV} = r\left(a'/w\right)$$

where r is the radioactivity activity concentration (kBq/mL) measured by the PET scanner within a ROI, a' is the decay-corrected amount of injected radiolabeled FDG (kBq), and w is patient weight [7]. Moreover, the maximum standardized uptake value (SUVmax) is the maximum number of counts within the pixels in a ROI and can be considered the actual semiquantitative measure useful in assessing ^{18}F-FDG rate of uptake in tissues.

A SUVmax cutoff value of 2.5 is commonly used to differentiate between benign and malignant lesions in PET/CT [8]; however, there are a significant number of false positives (due to inflammatory diseases) and false negatives (due to low-grade malignancies) [9]. It is necessary to state that, in oncology ^{18}F-FDG PET is generally assessed using visual criteria, looking for a focal area of increased uptake that can be compatible with malignancy, in the clinical context [10].

1.4 Clinical Indications

1.4.1 Differentiation Between Benign and Malignant Lesions

For its peculiar molecular properties, the ^{18}F-FDG is successfully employed in the differential diagnosis between malignant and benign lesions, or in assessing the metabolism of uncertain findings at conventional radiologic imaging. ^{18}F-FDG PET/CT can be useful for the characterization of enlarged lymph nodes, in the differential diagnosis among benign and malignant lesions of the bones and soft tissues. One of the most important field of applications of ^{18}F-FDG PET is the evaluation of solitary lung node: to date, the ^{18}F-FDG PET/CT allows to simultaneously evaluate the metabolism of the lung nodes and to depict, by the measurement of the SUVmax, which can improve the visual assessment of PET data in a clinical context [11]. In particular, it has been showed that a SUVmax > 2.5 is frequently asso-

ciated with a possibility of malignant nature of lung nodules. However, correlative CT imaging can also improve the specificity of PET imaging, allowing the concurrent possibility to describe morphologic findings as size, margins, eccentric calcifications or to ensure the contrast enhancement, when administered [9]. Anyway, the metabolic depiction of the pulmonary lesion is a significant information, especially for those lung nodes without evident radiographic characteristics of malignancy (Fig. 1.4). Conversely, nuclear medicine physicians cannot exclude the possibility of malignancy in some histological types of lung cancer, without significant glucose metabolism, as for bronco-alveolar carcinoma [12]: the accurate knowledge of the CT diagnostic criteria is of utmost importance, allowing to consider the PET/CT as a unique, hybrid, single session, whole body imaging modality with a useful overall diagnostic accuracy.

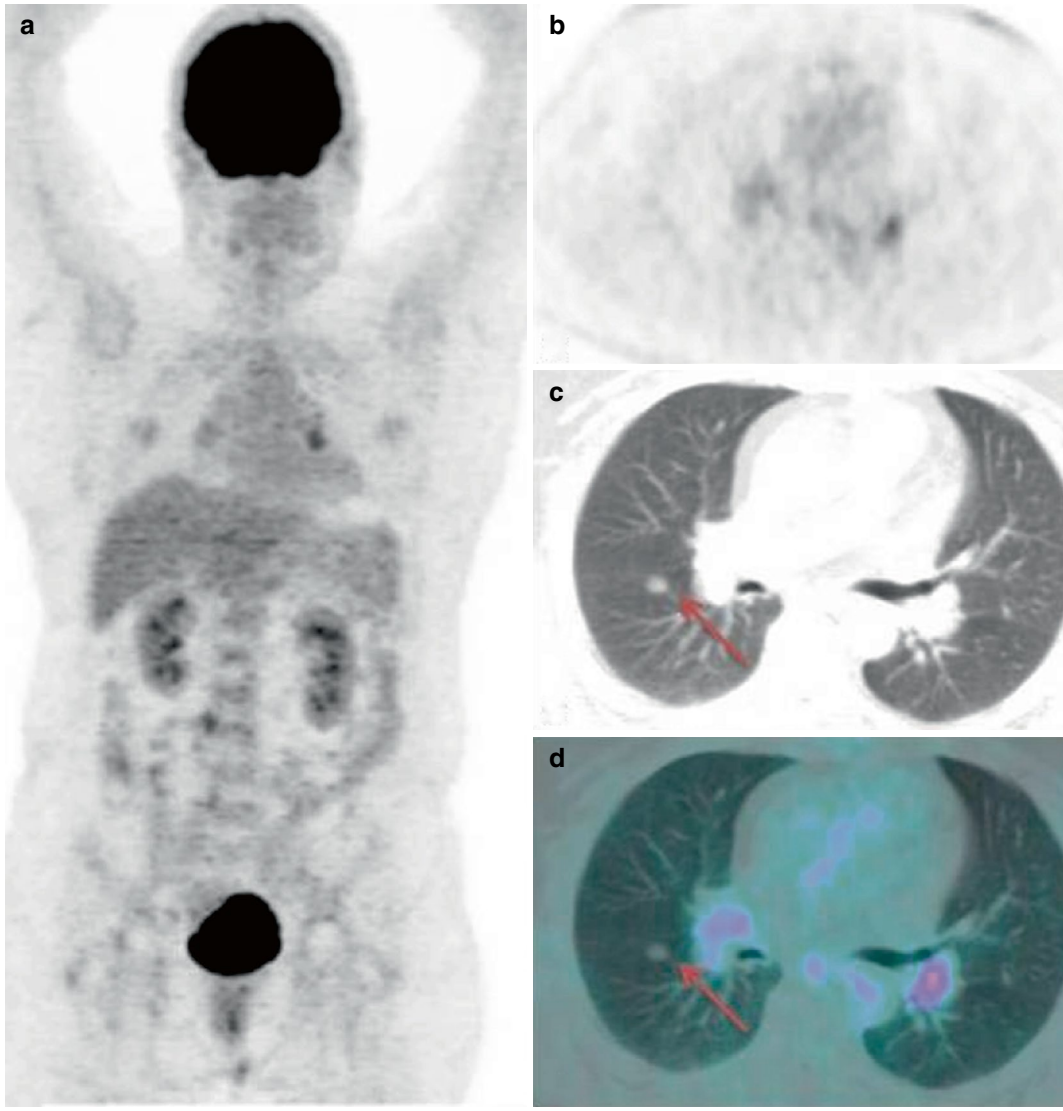

Fig. 1.4 Metabolic evaluation of a node in the right lung. PET 3D maximum intensity projection (**a**) and corresponding axial PET view (**b**) do not show significant uptake in the lesion. Axial CT (**c**) and PET/CT (**d**) views display a 1-cm wide node with regular margins and without characteristics of malignancy

1.4.2 Unknown Primary Tumor

Unknown primary tumors are a heterogeneous group of metastatic malignancies in which the primary tumor could not be detected despite diagnostic evaluation. Generally, these tumors are characterized by the presence of a metastatic lymph nodal disease, evident at conventional imaging (CT and/or MRI), with positive histological exam for malignant cells and no evidence of the primitive lesion [10]. The unknown primary tumors are aggressive diseases, with a poor survival, ranging from only 2–10 months from the diagnosis. Anyway, it can be hypothesized that the detection of the primary tumor may optimize treatment planning and, therefore, patient prognosis [13]. Despite a low diagnostic performance of ^{18}F-FDG PET/CT in detecting unknown primary tumors (Fig. 1.5), ranging from 25% to 43% in several meta-analysis [14], this diagnostic tool

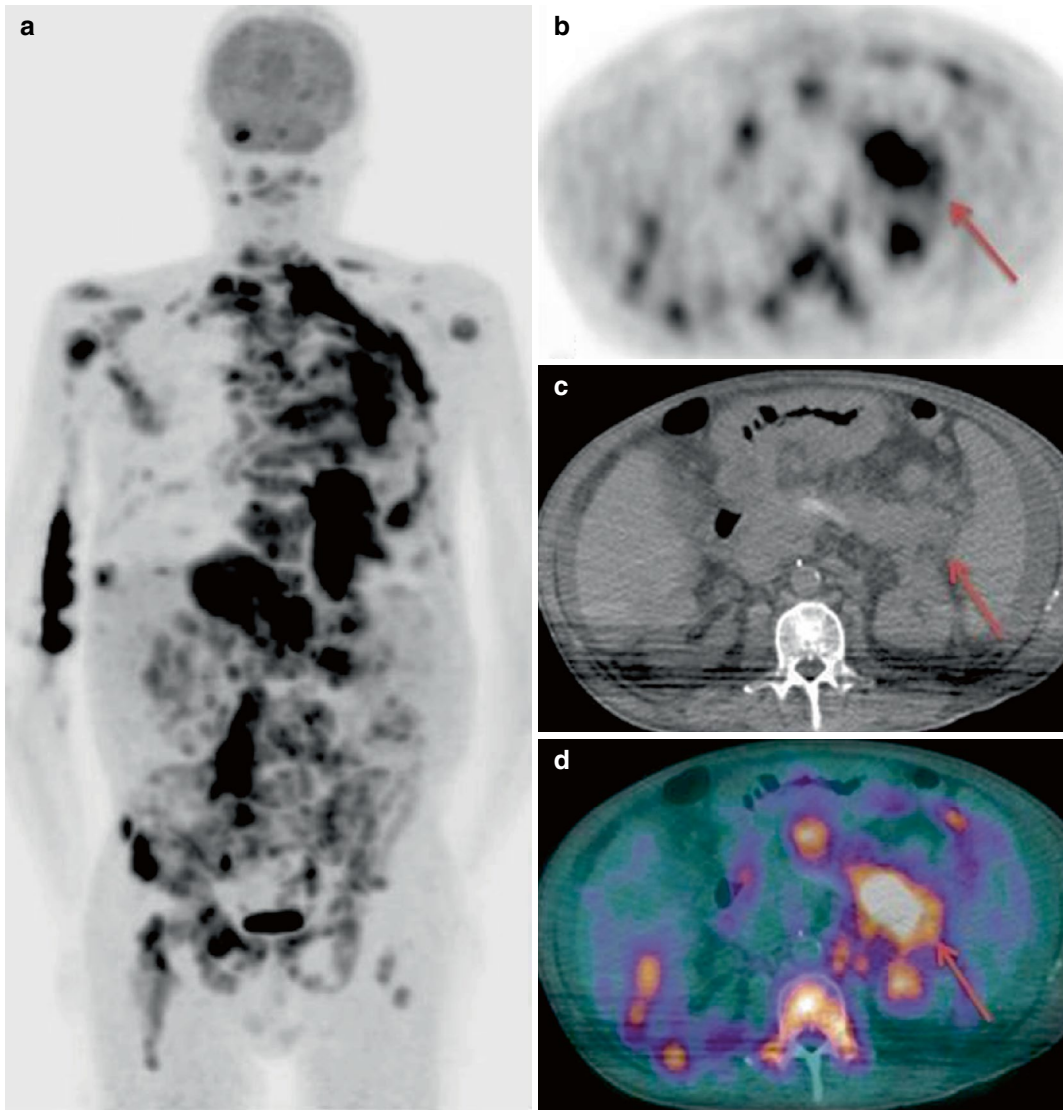

Fig. 1.5 Patient with multiple metastases of unknown primary tumor. ^{18}F-FDG 3D PET maximum intensity projection (**a**) shows multiple areas of pathologic tracer uptake in the brain, lungs, skeleton, thorax, and abdomen. Axial PET (**b**), CT (**c**), and PET/CT (**d**) views show focal and intense uptake in the tail of the pancreas (*final histological diagnosis: pancreas carcinoma*)

should be considered as first-line imaging method, due to the challenge to ensure the diagnosis with CT and to the very poor diagnostic accuracy of conventional imaging on this topic.

1.4.3 Staging

One of the main indications for ^{18}F-FDG PET/CT is the staging of patients with known malignancies, due to the capability in assessing tumor extension, lymph node metastases, and bone secondary lesions [15]. In fact, the hybrid PET/CT evaluation, with and without contrast media administration, also provides in a single whole body scan to rapidly obtain information regarding the primitive tumor and metastases, in order to choice the best therapeutic approach.

Indications for ^{18}F-FDG PET/CT during the staging of solid tumors include, but are not limited to, the following: lung cancer [16], locally advanced breast cancer (Fig. 1.6) [17], sarcoma [18], lymphomas (Fig. 1.7) [19], colon cancer [20], gynecological malignancies [21], and other kinds of tumor with high grade of glucose metabolism which potentially can be radically treated. ^{18}F-FDG PET-CT can also be used as a problem-solving tool to establish the baseline staging before commencing treatment in gastro-intestinal stromal tumors [22] and in head and neck cancer and prior to radical nodal resection in patients with suspicion of metastatic melanoma (Fig. 1.8) [23].

^{18}F-FDG PET/CT is also a valid guide to biopsy of suspected secondary bone lesions from somatic tumors [24] or in detecting the best site to perform biopsy. In fact, ^{18}F-FDG PET/CT has the advantage to accurately differentiate viable from nonviable tissues. This feature can reduce inconclusive biopsy results by specifically targeting areas of viability showing high rate of glucose metabolism [25].

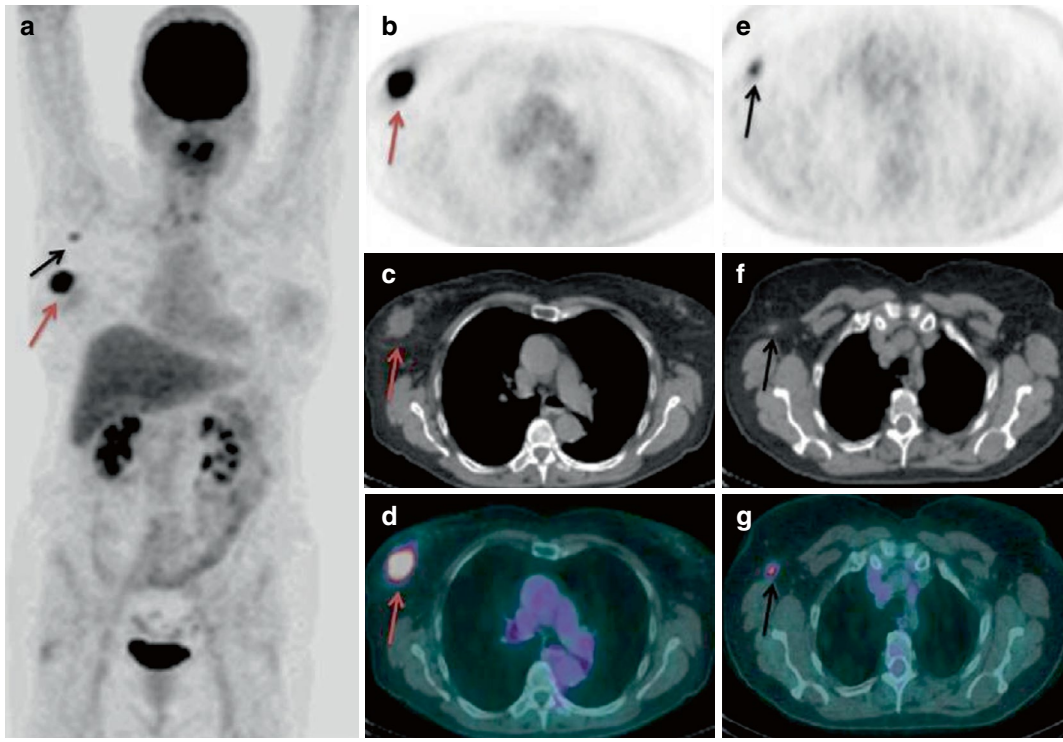

Fig. 1.6 A 56-year-old woman examined for staging locally advanced breast cancer. PET 3D maximum intensity projection (**a**) shows pathologic uptake in the upper outer quadrant of the right breast (*red arrow*) and a further area of uptake in the ipsilateral axilla (*black arrow*), as evident in corresponding axial PET views (**b**, **e**). The uptake was linked to a 3.2-cm-wide node in the breast and to a 1-cm-wide metastatic lymph node, as showed in corresponding CT (**c**, **f**) and PET/CT views (**d**, **g**)

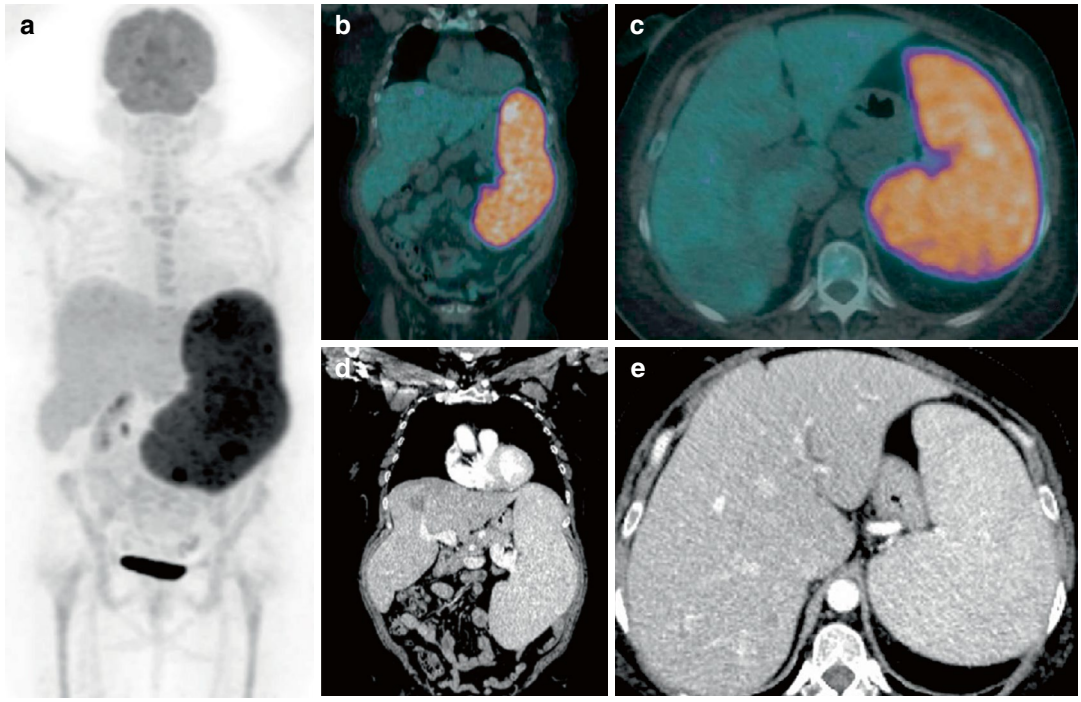

Fig. 1.7 In a patient with splenic lymphoma, PET 3D maximum intensity projection (**a**) shows abnormal tracer uptake in the spleen, in association with splenomegaly, as evident in PET/CT (**b**, **c**) and contrast-enhanced CT (**d**, **e**) coronal and axial views

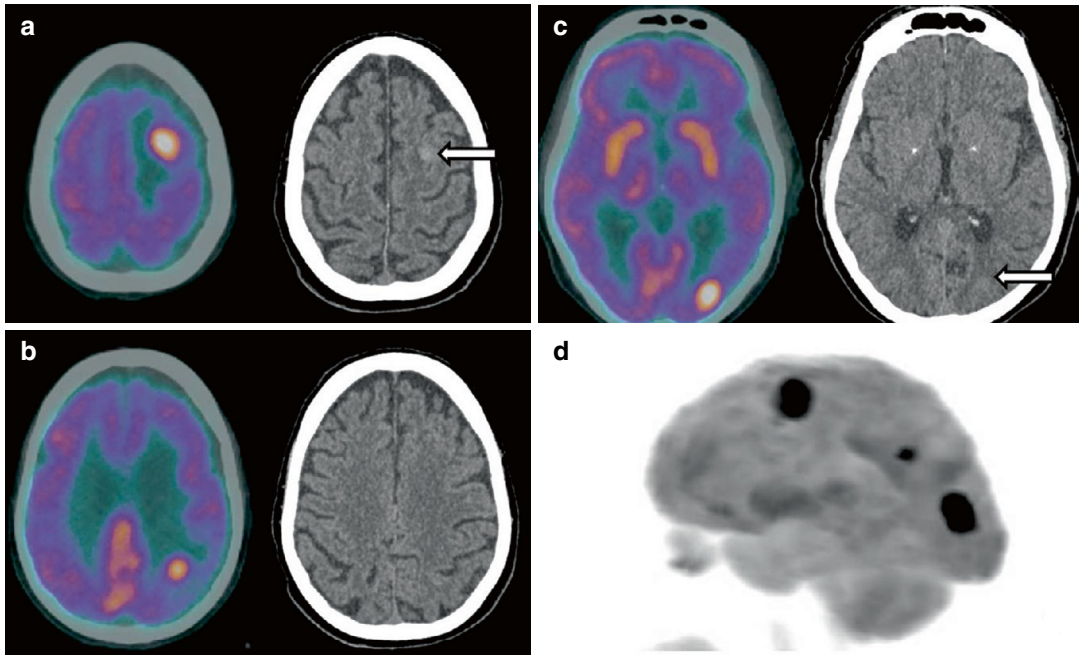

Fig. 1.8 In a patient with dorsal melanoma, axial PET/CT and CT views (**a**–**c**) show three foci of abnormal ^{18}F-FDG uptake in subcortical frontal, parietal, and occipital regions of the left cerebral hemisphere, due to hyperdense lesions (arrows), also evident in PET 3D maximum intensity projection of the brain (**d**)

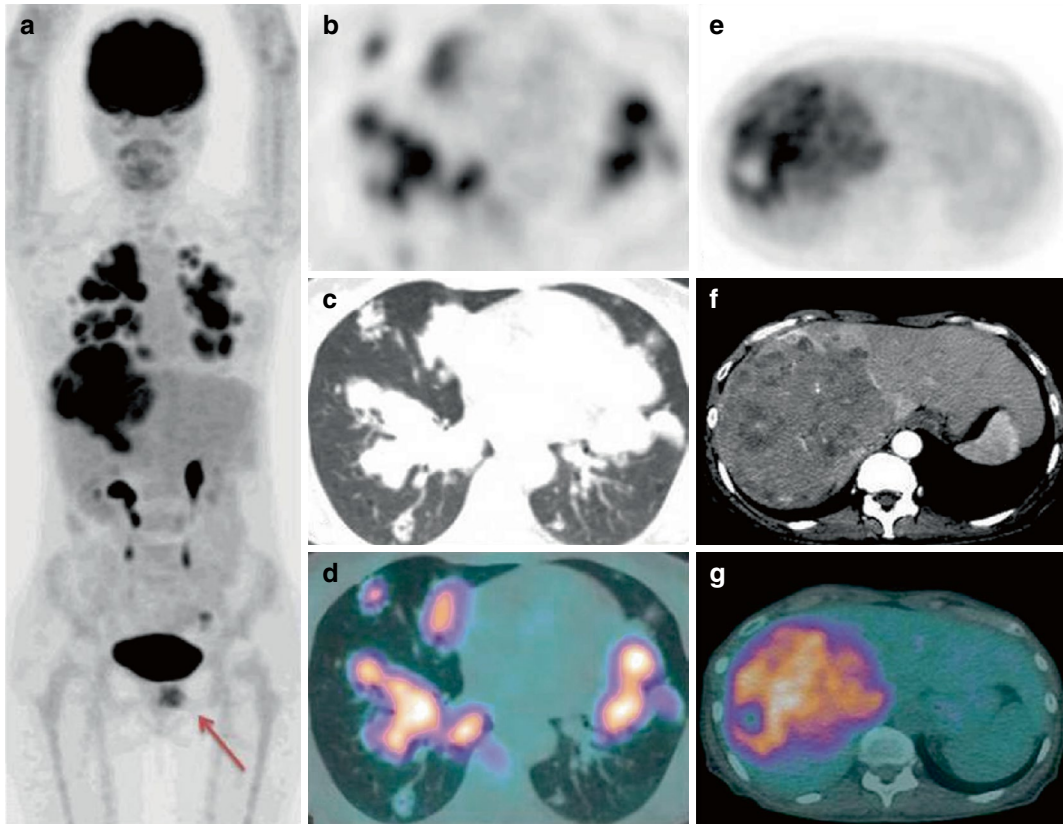

Fig. 1.9 Restaging in a 55-year-old patient with ovarian cancer and rising level of Ca-125, previously submitted to surgical intervention of isteroannessiectomy. PET 3D maximum intensity projection (**a**) shows pathologic uptake in the pelvis (*red arrow*) with multiple metastases in lungs (**b**, **c**, **d**) and liver (**e**, **f**, **g**), as evident in axial PET, CT, and PET/CT details

1.4.4 Restaging

^{18}F-FDG PET/CT is also useful in detecting tumor recurrence in patients with solid tumors previously treated for curative intent. The diagnostic performance of the exam is accurate especially in patients with rising tumor markers [26], suggestive for tumor relapse. Other tumors which can be evaluated during this phase are urological malignancies [27] and ovarian (Fig. 1.9) and esophageal cancer [28]. Also in this clinical setting, ^{18}F-FDG PET/CT has proven to be more accurate modality than CT for assessment of recurrence [29].

1.4.5 Assessment of Response to Therapy

Being an in vivo marker of tumor growth and vitality, the ^{18}F-FDG is useful for characterization of cancer cells metabolism during the time, especially for evaluating the response to therapy (chemotherapy and/or radiotherapy). In oncology, this approach can be directly applied in evaluating disease progression or in detecting the reduction of tumor metabolism [30], allowing to exceed limits of conventional anatomical imaging (Fig. 1.10).

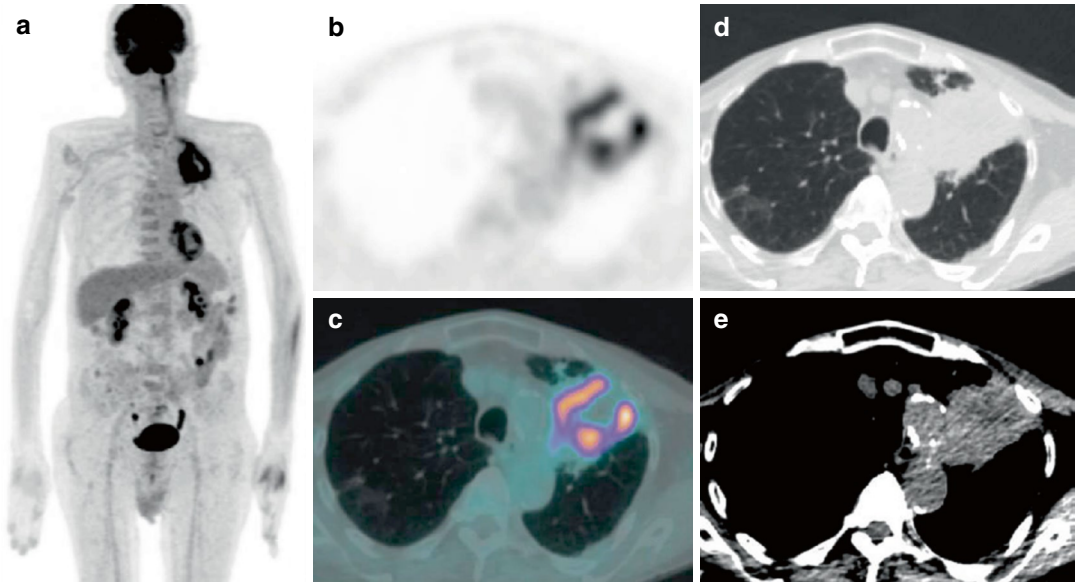

Fig. 1.10 A patient examined 3 months after radiotherapy for lung cancer. PET 3D maximum intensity projection (**a**) shows pathologic tracer uptake in the upper lobe of left lung, with internal core of hypometabolism due to post-actinic necrosis, as evident in axial ^{18}F-FDG PET (**b**) and PET/CT (**c**) views. Relative CT views (**d**, **e**) confirm a lung lesion with irregular borders and pleural infiltration

On this topic, the "*interim PET*" with ^{18}F-FDG, and its comparison with the "*baseline PET,*" has become a milestone for the imaging of lymphomas. In particular, in patients with Hodgkin lymphoma, the *interim PET* after two courses of standard therapy allows to ensure the response to therapy and to predict the survival-free progression of patients. For example, a negative "*interim PET*" determines the prosecution of the standard therapy and is associated with a complete remission of the disease (Figs. 1.11 and 1.12). Instead, the minority of patients with Hodgkin lymphoma presenting a positive "*interim PET*" need intensification of second-line chemotherapy with the eventual addition of radiotherapy [31] and present a poor prognosis (Fig. 1.13).

Beyond hematology, the principle of using the molecular properties of ^{18}F-FDG as marker of chemosensitivity can be applied to all solid tumors with high rate of glucose metabolism (Fig. 1.14). Moreover, this diagnostic tracer can also be useful in assessing response to radiotherapy (Fig. 1.15) [32].

1.4.6 Detection of Tumor Recurrence

An important feature of ^{18}F-FDG PET/CT is the capability to detect tumor recurrence of all tumors with high rate of glucose metabolism. The added value provided by the molecular properties of ^{18}F-FDG is the early diagnosis of local relapse or the identification of secondary metastases which can lead to an optimal assessment of small secondary lymph node lesions or bone metastases, also before the osseous remodeling.

This property can help clinicians in the early diagnosis of tumor recurrence and in promptly planning the best therapeutic approach, before these lesions can be detected at conventional imaging (Fig. 1.16).

1.4.7 Radiation Therapy Planning

The appropriate selection and delineation of target volumes prior to perform radiotherapy in oncology, generally performed with contrast-

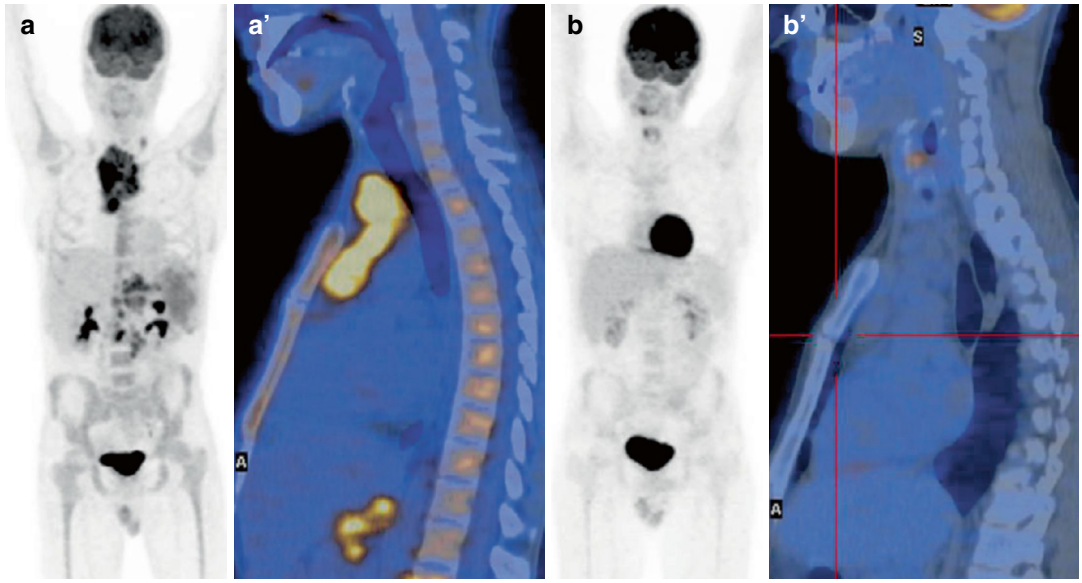

Fig. 1.11 "*Baseline*" (**a**, **a′**) and "*interim* (**b**, **b′**) *^{18}F-FDG PET/CT*" showing a patient with mediastinal bulky Hodgkin lymphoma before and after two cycles of *adriamycin–bleomycin–vinblastine–dacarbazine* (ABVD). The complete absence of uptake in the mediastinum in the *interim PET* (**b**, **b′**), assessed by visual analysis, allows to diagnose early response to therapy and to predict a complete remission of lymphoma. Interestingly, a residual hypodense tissue is still evident in the upper mediastinum in sagittal PET/CT view of the *interim PET/CT* (**b′**), not expressing metabolic activity

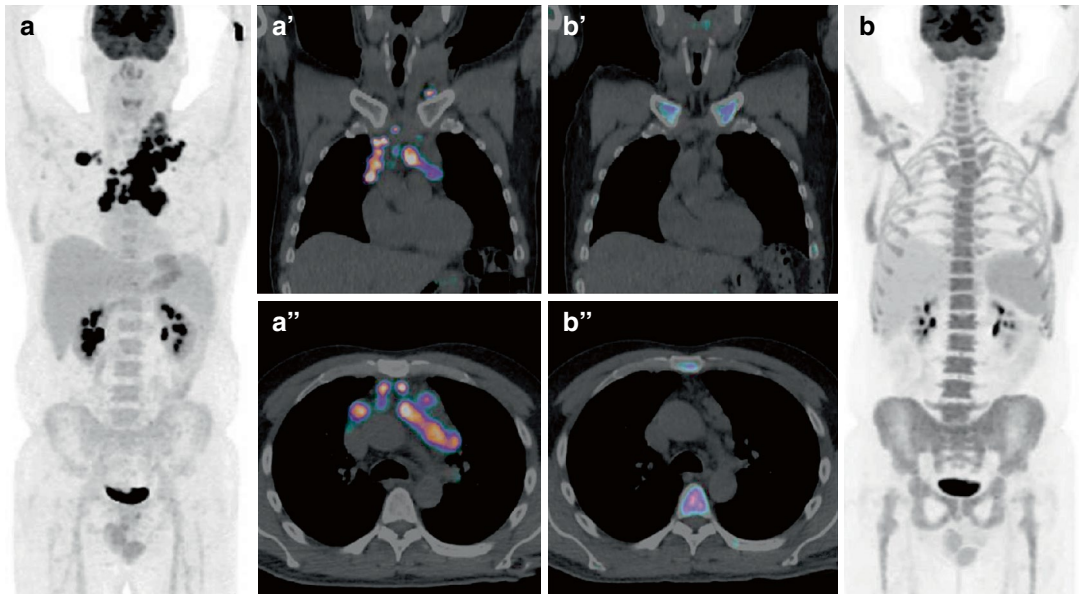

Fig. 1.12 In a patient with Hodgkin lymphoma, "*Baseline*" ^{18}F-FDG PET/CT (**a**, **a′**, **a″**) shows pathologic tracer uptake in cervical and mediastinal lymph nodes. After two cycles of *adriamycin–bleomycin–vinblastine–dacarbazine* (ABVD), the "*interim*" ^{18}F-FDG PET/CT (**b**, **b′**, **b″**) shows residual lymph nodes in mediastinum, without significant metabolic activity, diagnosing early response to therapy

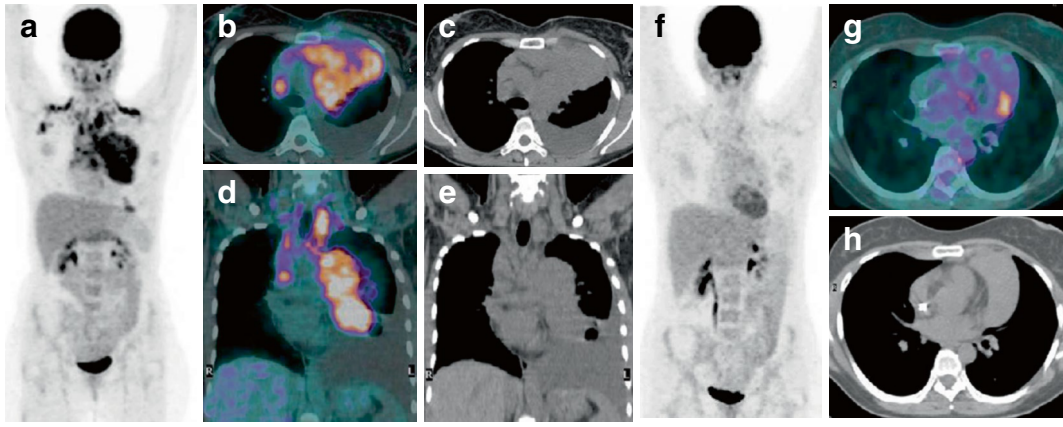

Fig. 1.13 "*Baseline* (**a**–**e**) *PET/CT*" of a patient with Hodgkin lymphoma showing a bulky mediastinal mass with other cervical lymph nodes, expressing pathologic tracer uptake. Despite the significant reduction of the volume lesion after two cycles of *adriamycin–bleomycin–vinblastine–dacarbazine* (ABVD), the "*interim PET/CT*" (**f–h**) displays a single area of focal uptake in the residual lesion of upper mediastinum, indicative of failed response to therapy

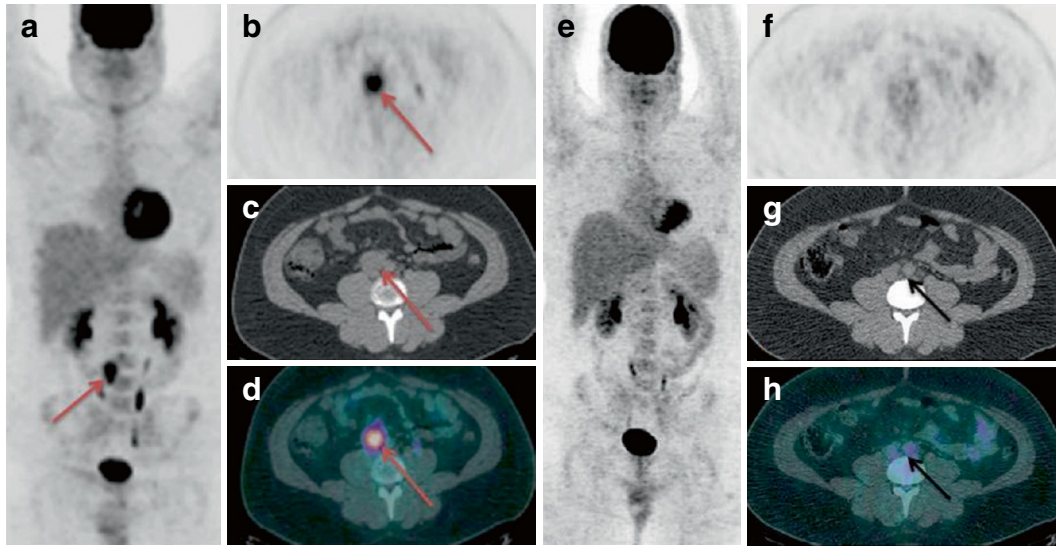

Fig. 1.14 A 23-year-old patient previously submitted to excision of seminoma of the right testicle was examined by PET/CT, showing pathologic tracer uptake in a 2.8-cm-wide abdominal, retrocaval lymphadenopathy (red arrow), evident in MIP (**a**) and axial PET (**b**), CT (**c**), and PET/CT (**d**) views. After the end of chemotherapy, a further exam allowed to diagnose a residual lymphatic tissue without meaningful metabolic activity, indicative of response to therapy, as evident in MIP (**e**) and axial PET (**f**), CT (**g**), and PET/CT (**h**) views

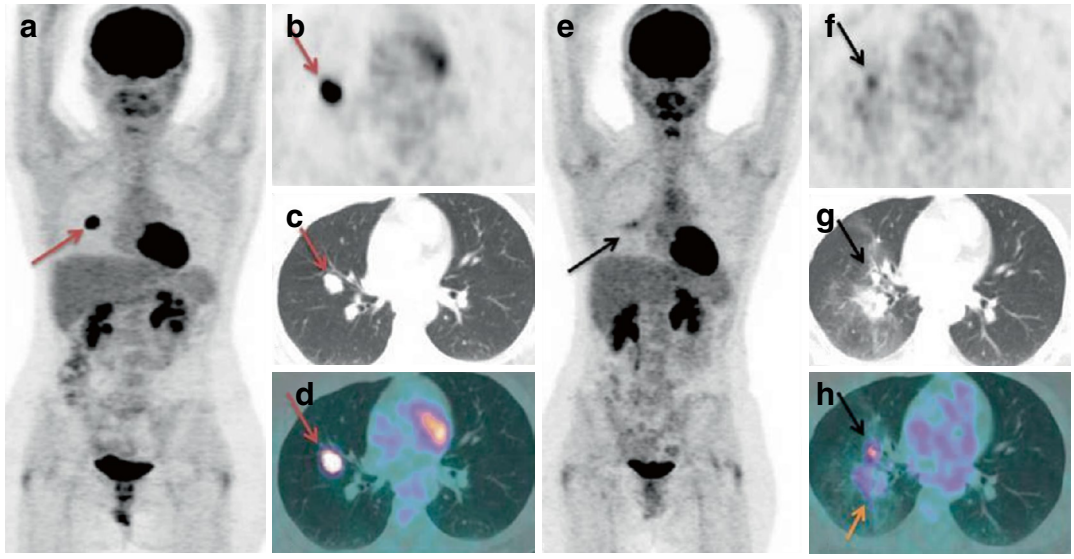

Fig. 1.15 PET 3D maximum intensity projection (**a**) shows pathologic tracer uptake in a lung node, 2.8 cm wide (*red arrow*), better displayed on correlative axial PET (**b**), CT (**c**), and PET/CT (**d**) views. Histological exam diagnosed lung carcinoma. Six months after radiotherapy (**e–h**), the volume lesion was considerably reduced with mild metabolic activity, indicative of residual tumor (*black arrow*). The *yellow arrow* in axial PET/CT view (**h**) shows low, physiological uptake in radiation-induced lung inflammation

enhanced CT or MRI, is of utmost importance. The intrinsic advantage of PET imaging is the possibility to delineate the metabolically active part of tumors, improving the choice and the extension of the radiotherapy field. Naturally, limits of this tool are the low spatial resolution, which has been recently considerably improved by the development of novel PET/CT and hybrid PET/MRI scanners.

For lung cancer, the ^{18}F-FDG PET/CT for radiation planning has added biological information in defining the gross tumor volume and the eventual concomitant nodal disease. For example, the accurate target delineation between tumor and atelectasis is achievable by using PET and CT imaging simultaneously [33]. Several articles recently published propose the use of PET/CT for radiotherapy planning in esophageal cancer, head and neck carcinoma, and anal tumors [34–36].

1.4.8 Inflammation and Infection

In addition to its established role in oncological imaging, ^{18}F-FDG PET/CT can also have clinical utility in evaluating infection and inflammation. In fact, this diagnostic tool can identify the source of inflammation (Fig. 1.17) or infection (Fig. 1.18), more accurately than conventional anatomical imaging techniques, such as CT and MRI. Moreover, ^{18}F-FDG PET/CT could map the extent of disease: for example, the involvement of bone tissue in case of osteomyelitis or *Charcot foot* (Fig. 1.19). Consecutive exams help to assess therapy response [37].

The advantages of PET/CT technology, in comparison with conventional SPECT or SPECT/CT imaging with ^{99m}Tc-labeled leukocytes [38], are due to a shorter duration of examination, higher spatial resolution, and noninvasive nature of scan (Fig. 1.20) [39].

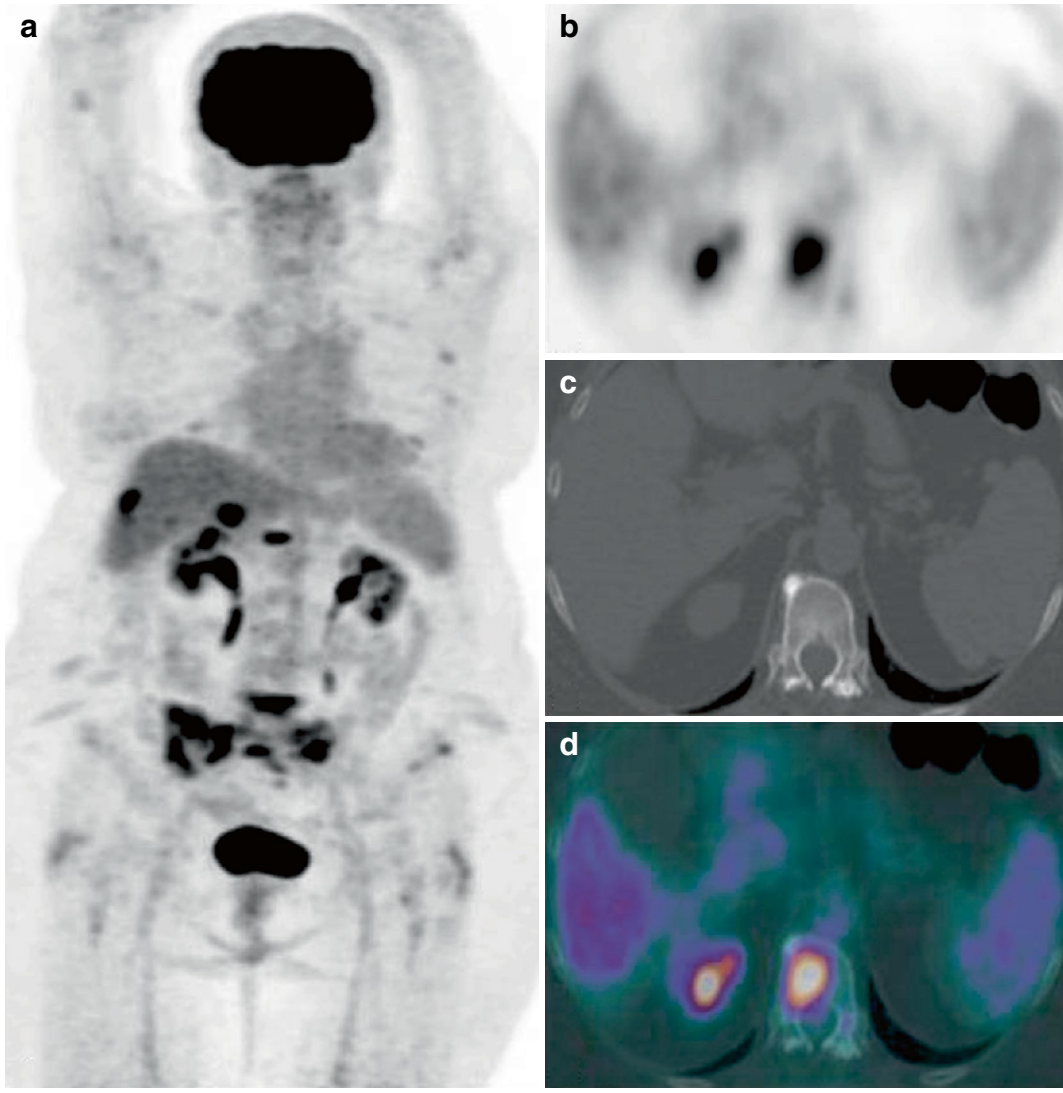

Fig. 1.16 ^{18}F-FDG PET 3D maximum intensity projection (**a**) shows several bone metastases and a hepatic lesion in a 61-year-old woman examined for restaging breast cancer. Axial PET detail (**b**) shows focal uptake in the 11th thoracic vertebra, without morphological alterations on the CT component of the exam (**c**, **d**)

Anyway, due to the lack of specificity of ^{18}F-FDG, recent studies are examining ^{18}F-FDG-labeled leukocytes PET/CT as a useful diagnostic tool to investigate inflammation and infection in soft-tissue imaging [40].

^{18}F-FDG PET/CT can show inflammatory activity in the aorta and major arteries in patients with active Takayasu arteritis (Fig. 1.21). The intensity of accumulation may decrease in response to therapy [41, 42].

Under study is the potential usefulness of ^{18}F-FDG PET/CT in the assessment of activity, staging, follow-up, and prognosis estimation of patients with chronic intestinal inflammatory disease as Crohn's disease [43] and ulcerative colitis [44].

Finally, ^{18}F-FDG PET/CT can be of help in diagnosis and assessment of response to therapy of invasive fungal infections [45, 46], tuberculosis [47], and other thoracic granulomatous diseases [48, 49].

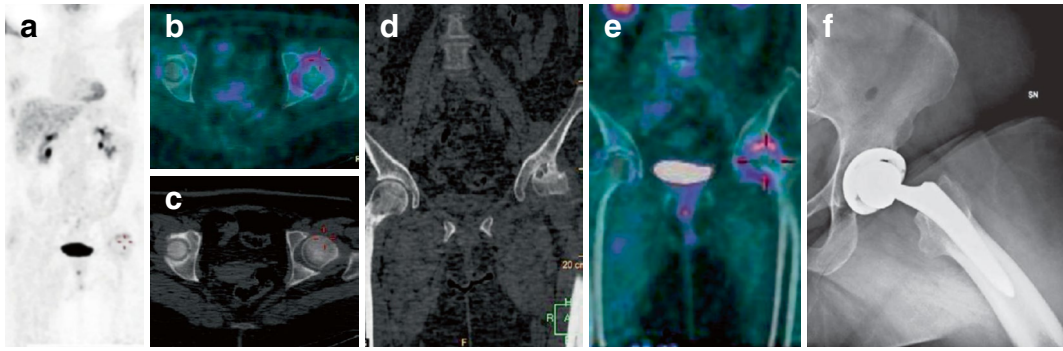

Fig. 1.17 ^{18}F-FDG PET 3D maximum intensity projection (**a**) shows diffuse uptake surrounding the head of left femur, due to inflammation, as evident in corresponding axial (**b**, **c**) and coronal (**d**, **e**) CT and PET/CT views. In particular, in coronal CT view (**d**) are evident the geodic lesions due to arthrosis. X-rays (**f**), performed after surgical intervention, confirm the correct femoral prosthesis insertion

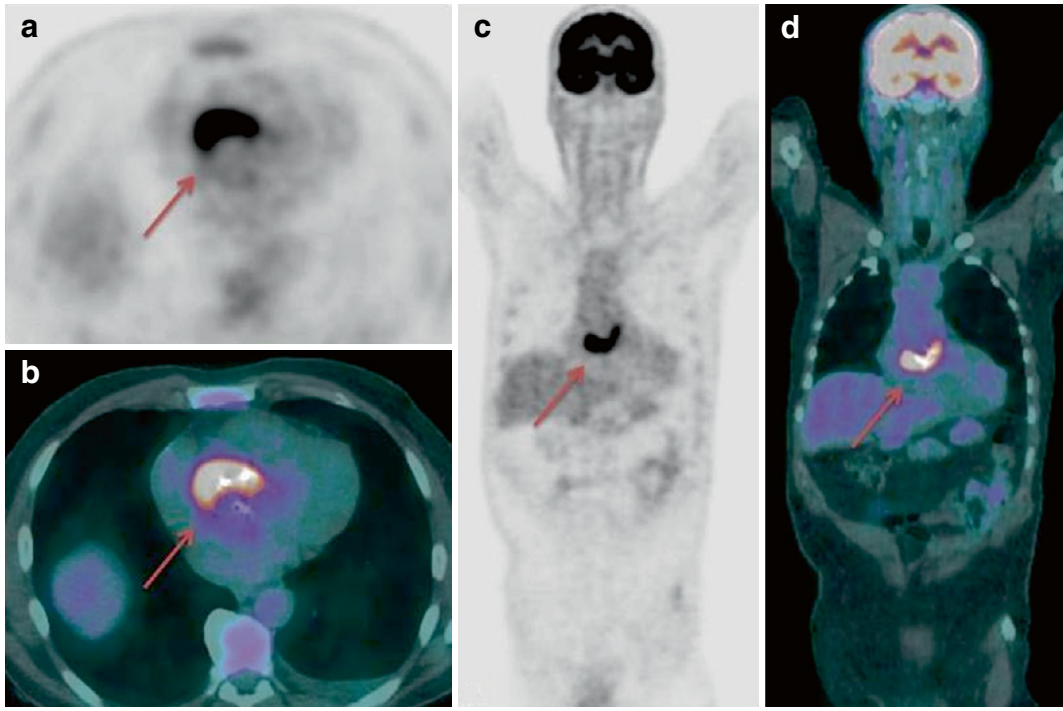

Fig. 1.18 A 57-year-old patient with prosthetic valve endocarditis: axial PET (**a**) and PET/CT (**b**) views, coronal PET (**c**) and PET/CT (**d**) views show high ^{18}F-FDG uptake around prosthetic aortic valve, indicative of infective endocarditis

1.4.9 Neuroimaging

^{18}F-FDG PET is able to visualize a *map* of the whole brain glucose metabolism, being normally enhanced in normal structures of white and gray matter.

In fact, the bio-distribution of ^{18}F-FDG in the brain regards gray and white matters, thalamus, caudate nuclei, and cerebellum. The reduction of the uptake in these structures allows to recognize some neurodegenerative diseases, characterized by a typical pattern of deficit extension, generally

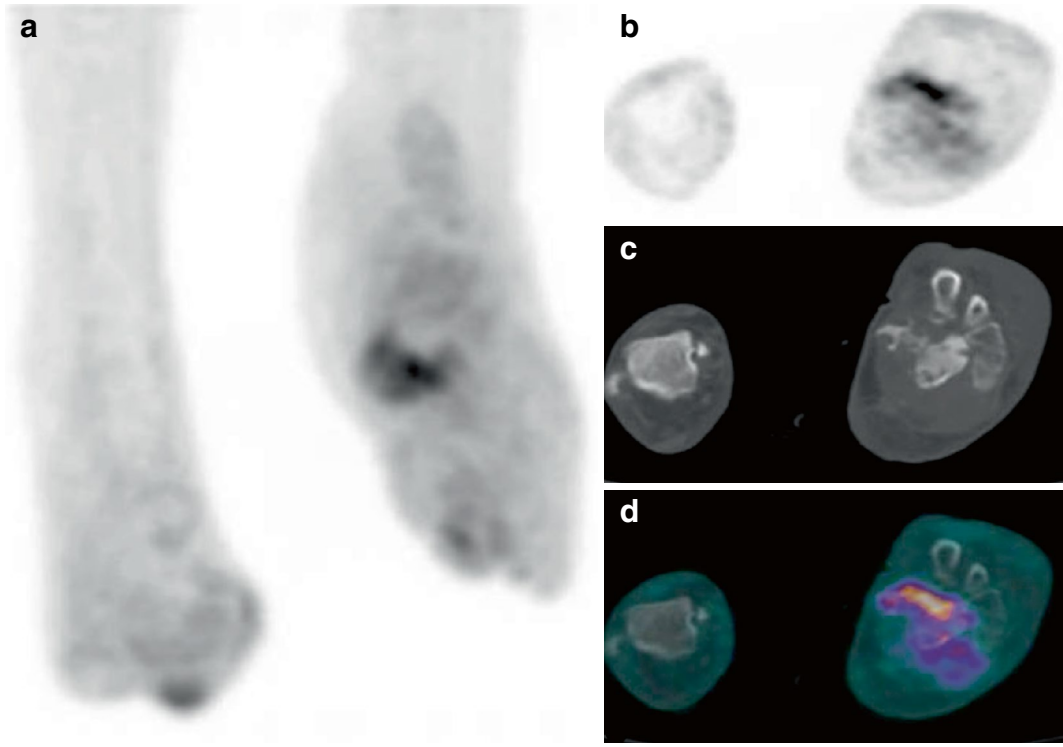

Fig. 1.19 ^{18}F-FDG PET/CT imaging in a diabetic foot: PET 3D maximum intensity projection (**a**) and PET axial view (**b**) show intense tracer uptake in the left tarsal region, with partial bone involvement, as evident in correlative axial CT (**c**) and PET/CT (**d**) views

before morphologic abnormalities can be observed on MRI. For the same reason, the CT component of the PET/CT, in neurological studies, is generally not useful, excepting data for attenuation correction and anatomical landmarks.

^{18}F-FDG PET can be a valid tool, according to clinical examination, in discriminating between several kinds of dementia: Alzheimer disease (AD) generally shows hypometabolism in the parietotemporal association area, posterior cingulate, and precuneus (Fig. 1.22); hypometabolism in the inferior parietal lobe and posterior cingulate/precuneus is a predictor of cognitive decline from mild cognitive impairment to AD dementia. Conversely, a deficit of uptake in frontotemporal region is indicative of frontotemporal dementia. Moreover, seriate scans can offer the possibility to evaluate the disease progression and its evolution.

However, we must also consider the recent development and commercial availability of β-amyloid specific tracers (see Chap. 8), which are replacing ^{18}F-FDG scans in patients with suspicion of AD or mild cognitive impairment, due to the better tracer specificity and predictive value. However, brain ^{18}F-FDG PET still plays a role in the management of patients with dementia, also allowing global evaluation of cortical, cerebellar, and subcortical regions of the brain (Fig. 1.23).

Concerning the imaging of movement disorders, ^{18}F-FDG cannot easily detect the reduction of metabolism in the striatum, due to its high rate of physiological bio-distribution in this structure, also in comparison with ^{18}F-DOPA (see Chap. 2) [50]. ^{18}F-FDG PET can only support the clinical diagnosis of Parkinsonian syndromes, allowing the characterization of specific uptake patterns when the differential diagnosis between supra-

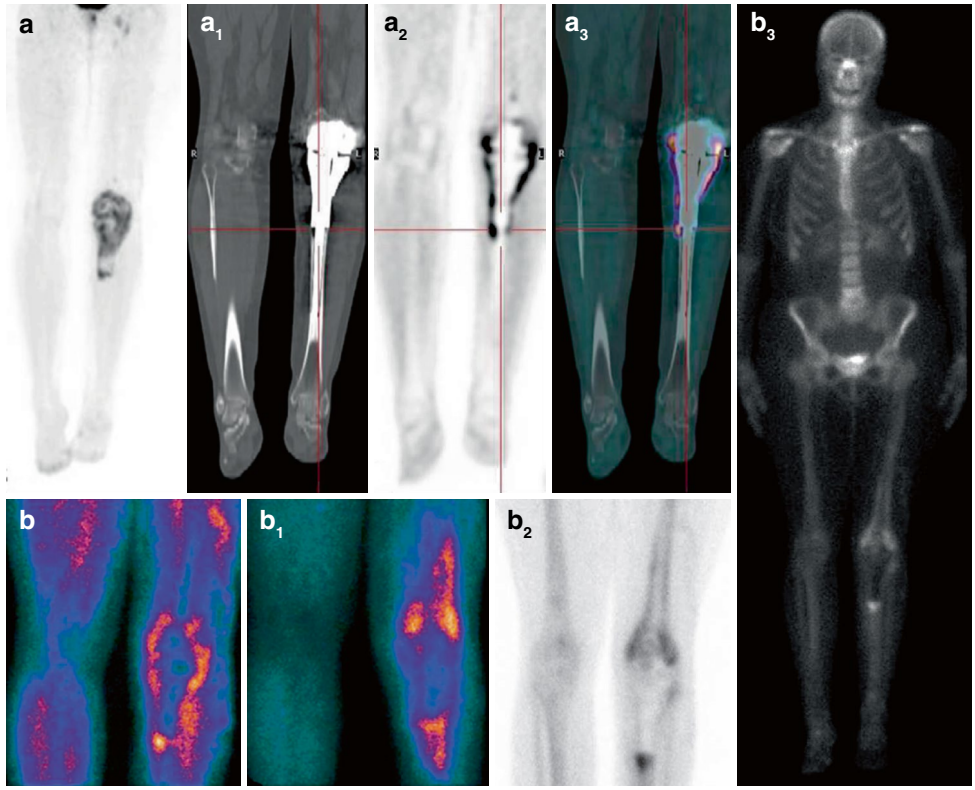

Fig. 1.20 ^{18}F-FDG PET 3D maximum intensity projection (**a**), coronal CT (**a$_1$**), PET (**a$_2$**), and PET/CT (**a$_3$**) views show intense pathologic tracer uptake surrounding a prosthesis of the left knee. Triphasic planar scintigraphy with ^{99m}Tc-labeled leukocytes (**b**, **b$_1$**, **b$_2$**, and **b$_3$**) confirms the diagnosis of soft tissue infection around the prosthetic joint. This case summarizes the better power resolution limit of PET/CT in comparison with a higher specificity of scintigraphic imaging with ^{99m}Tc-labeled leukocytes

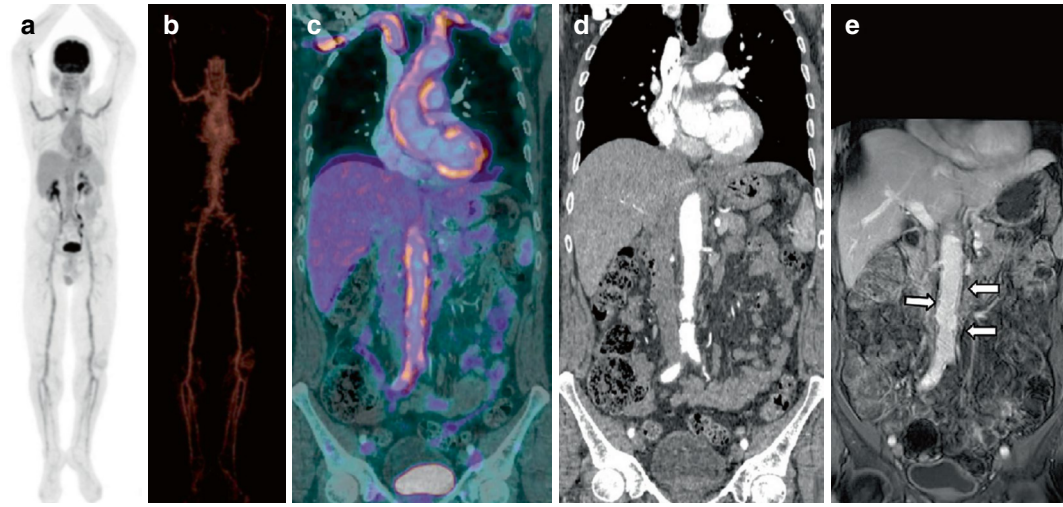

Fig. 1.21 Patient with Takayasu arteritis. ^{18}F-FDG PET 3D maximum intensity projection (**a**) and PET 3D volume rendering (**b**) show intense and pathologic tracer uptake in vascular structures of mediastinum and major arteries of the body. Coronal PET/CT (**c**) and contrast-enhanced CT (**d**) display the uptake in the abdominal aorta and iliac arteries. MRI (**e**) shows abdominal aortic wall thickening (*arrows*). *Credits to Rosanna Tavolaro (MD) and Mario Leporace (MD), Department of Nuclear Medicine and Theranostics, Mariano Santo Hospital, Cosenza*

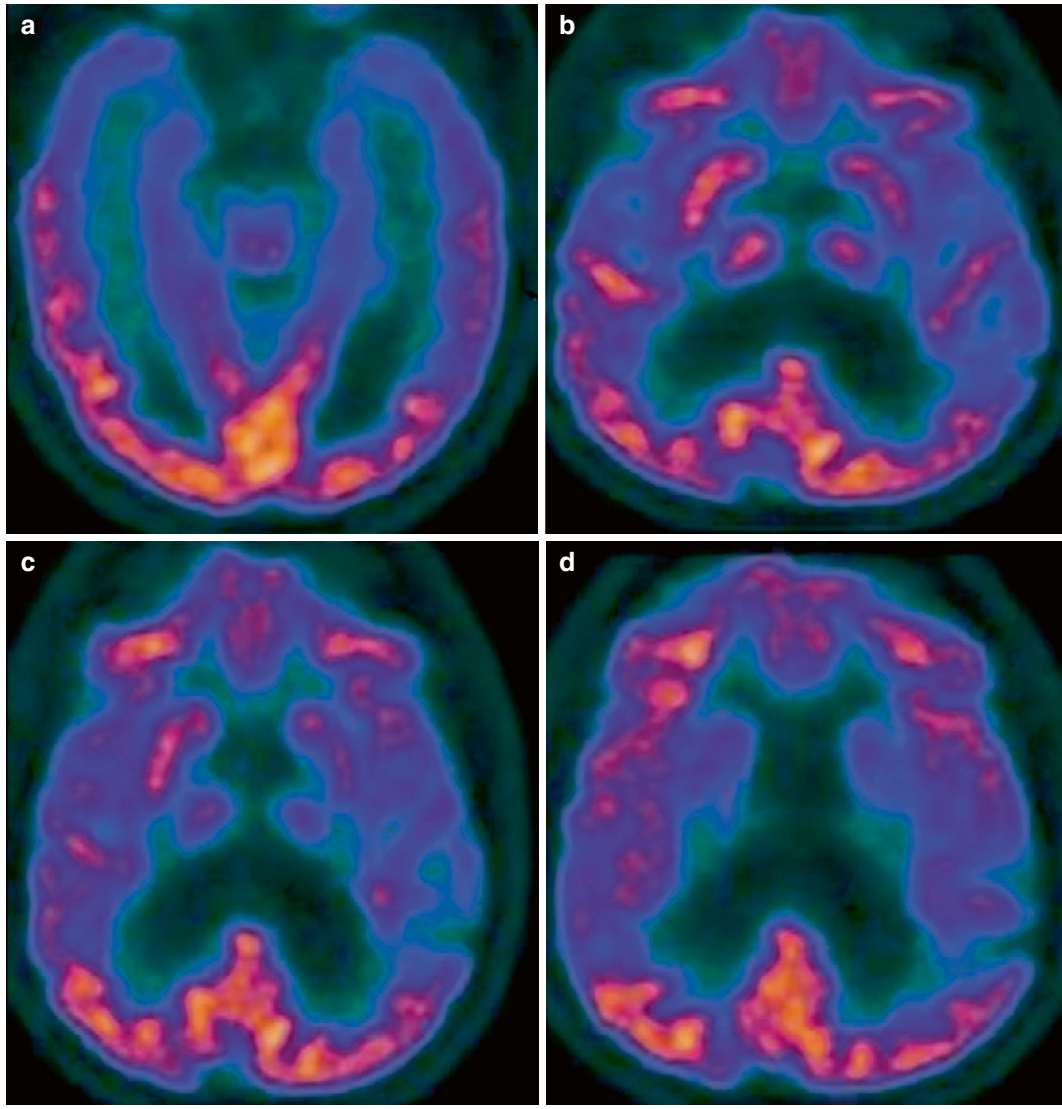

Fig. 1.22 Axial PET views (**a–d**) showing bilateral parietotemporal deficit of glucose metabolism in a patient examined for suspicion of Alzheimer's disease

nuclear progressive palsy, multisystemic atrophy, and cortico-basal degeneration is uncertain [51]. Consequently, the attention of the researchers is focused on the potential usefulness of brain ^{18}F-FDG PET in the differential diagnosis of Parkinsonian syndromes or in detecting, in a minority of patients with Parkinson's disease, the related *dementia complex* [52].

Other potential applications of brain ^{18}F-FDG PET are linked to its capability to detect epileptogenic foci. In particular, *ictal* ^{18}F-FDG PET, with tracer administration occurring during the crisis, has proven to be very sensitive in identifying the temporal or extra-temporal epileptogenic focus, despite its difficult reproducibility [53].

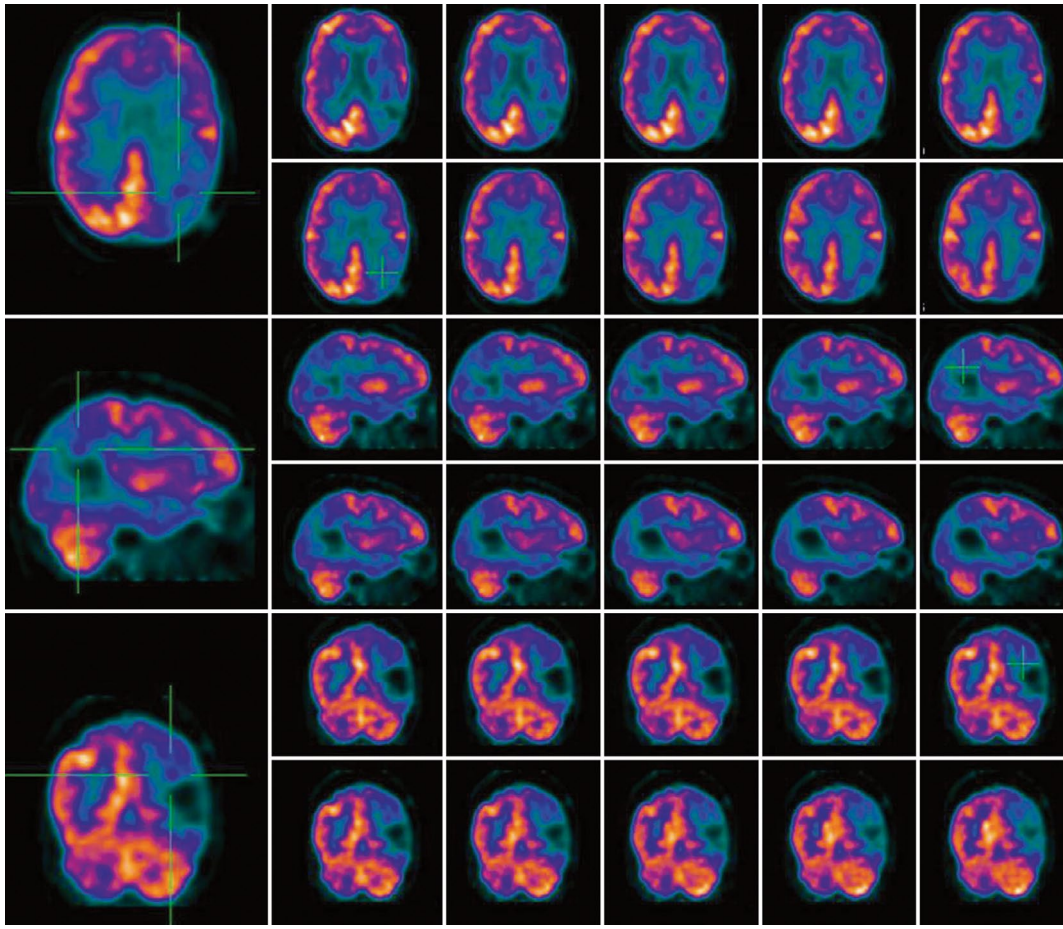

Fig. 1.23 Multiplanar PET evaluation of a patient with a past history of stroke in the left parietal region. The brain ^{18}F-FDG PET was performed 2 years after the ischemic injury and shows deficit of glucose metabolism in the left parietal region, in association with deficit of ^{18}F-FDG uptake in the contralateral cerebellar hemisphere (*crossed cerebellar diaschisis*)

As a future trend, due to the versatility of the tracer, we can consider an emerging indication of ^{18}F-FDG PET the study of autoimmune encephalitis, due to the challenge to depict the site of neuronal inflammation (Fig. 1.24) and to monitor the response to therapy [54].

1.4.10 Myocardial Viability

The assessment of myocardial viability has become an important investigation in the management of patients with ventricular dysfunction following an ischemic event. The assessment of residual myocardial viability can be useful to individualize the management of patients and can help in deciding whether patients should receive surgical or medical treatment based on PET data or, alternatively, need to undergone revascularization. The ^{18}F-FDG "*myocardial*" PET is performed after a rest injection of the tracer, followed by a PET scan triggered with cardiac cycle, in order to avoid motion artifacts of the heart (see also

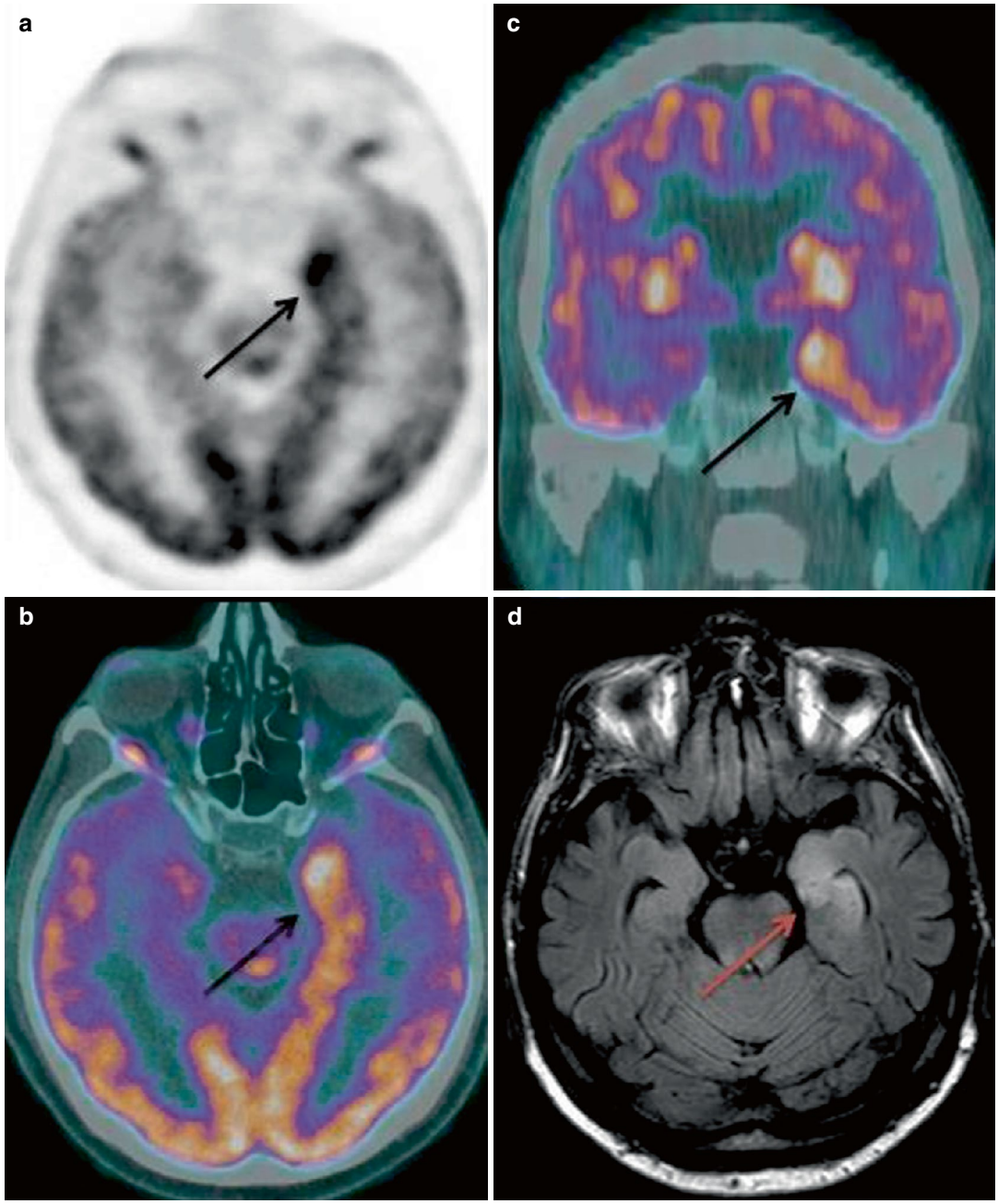

Fig. 1.24 In a 56-year-old patient with autoimmune encephalitis, axial ^{18}F-FDG PET view (**a**, black arrow) shows hypermetabolism in the left temporal lobe, as evident also in axial (**b**) and coronal (**c**) PET/CT views. Axial T2 FLAIR MRI (**d**) displays hyperintensity in the left hippocampus, due to the condition of encephalitis

Chap. 9). Anyway, for nuclear medicine physicians experienced in this field, the cornerstone to evaluate PET data is the myocardial perfusion imaging with SPECT, which is necessary to individuate regional myocardial hypoperfusion which can display ^{18}F-FDG uptake and therefore be susceptible of revascularization (Fig. 1.25).

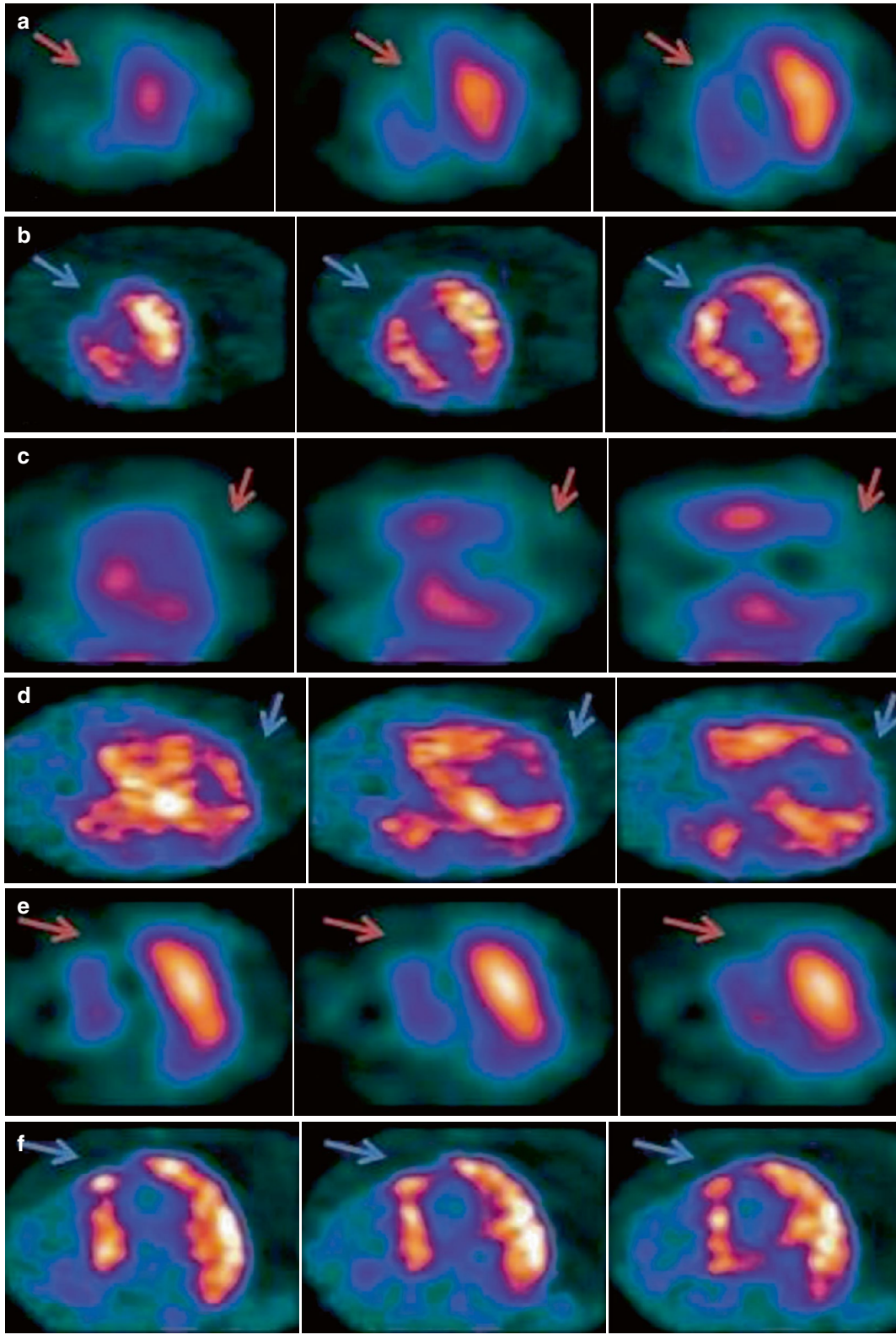

Fig. 1.25 Myocardial SPECT (**a**, **c**, **e**) shows perfusion deficit in the apex of the left ventricle; correlative myocardial PET with ^{18}F-FDG (**b**, **d**, **f**) displays tracer uptake in the apex, indicative of myocardial viability